ELSEVIER

Nuclear Instruments and Methods in Physics Research A 366 (1995) 120-128

NUCLEAR INSTRUMENTS & METHODS IN PHYSICS RESEARCH Section A

# Particle discriminator for the identification of light charged particles with CsI(Tl) scintillator + PIN photodiode detector

J. Gál [a,*], G. Kalinka [a], B.M. Nyakó [a], G.E. Perez [a], Z. Máté [a], G. Hegyesi [a], T. Vass [a], A. Kerek [b], A. Johnson [b]

[a] Institute of Nuclear Research, P.O.Box 51, H-4001 Debrecen, Hungary

[b] The Royal Institute of Technology, Physics Department Frescati, Stockholm, Sweden

Received 10 May 1995

**Abstract**

A particle discriminator exploiting the ballistic deficit effect for pulse shape discrimination has been developed for CsI(Tl) scintillator + PIN photodiode charged-particle detectors. The method is theoretically investigated and it is shown that the figure of merit of the particle separation is mainly governed by the absolute value of the differential quotient of the rise time dependent ballistic deficit. As the actual particle discriminator contains shaping amplifiers, baseline restorer, pile-up rejector and analog-to-digital converters, it directly accepts signals from a charge-sensitive preamplifier, and its outputs deliver the type and the energy of the particles in the form of eight-bit digital codes. The performance of the particle discriminator is characterised by the figure-of-merit measured as a function of the particle energy.

## 1. Introduction

The CsI(Tl) scintillation crystal is widely used for charged-particle discrimination, since its scintillation light is composed of a slow and a fast component, the amplitude ratio of which as well as the decay-time constant of the fast component vary with the type of the particle [1,2]. In our case the scintillation light is sensed by a PIN photodiode, which is connected to the input of a charge sensitive preamplifier described in Ref. [3]. Since the rise-time constant of such a preamplifier is equal to the decay-time constant of the scintillation light, the *particle-type* information is carried by the rise-time constant of the preamplifier output pulse.

Basically two techniques are used to exploit the particle discrimination capability of the crystal: the zero crossing [4-6] and the charge comparison methods [7,8]. The technique we have developed is principally a charge comparison method, but its realization differs from the usual ones in that it is based on the ballistic deficit phenomenon which is the amplitude degradation at the output of a pulse shaping circuit due to the finite rise time of the input pulse. The larger the rise-time constant to shaping-time constant ratio is, the larger the amplitude degradation will be. (Note that the pulse shape discriminator of Brooks [7] is practically based on the ballistic deficit phenomenon, although it is not mentioned in his article.) Due to the particle dependent amplitude ratio of the fast and slow components and the particle dependent decay-time constant of the fast component of the CsI(Tl) scintillation light, the ballistic deficit of a shaping circuit output pulse will be characteristic of the type of the particle.

In our particle discriminator unit (PDU) the measurement of the ballistic deficit for a given input pulse is realised by comparing the outputs of two shaping circuits having different shaping time constants, i.e. different ballistic deficits. For the comparison, the two signals are divided by each other [9-11] using an analog divider. Its output carries the *particle-type* information, while the output of the shaping circuit having the longer shaping time constant provides the *energy* of the particles.

## 2. Operating principle

### 2.1. Theoretical considerations

In this section we characterise the above mentioned pulse shape discrimination technique quantitatively. The ballistic deficit can be considered as an effect due to which the amplitude of the output pulse of a shaping circuit corresponds to only a fraction of the total charge $Q_t$ deliberated in the detector [12-14]. Denoting this fractional charge by $Q_p$, one can introduce the normalised partially collected charge $F$ given by the ratio

* Corresponding author. Tel. +36 52 417 266, fax +36 52 416 181.


SSDI 0168-9002(95)00560-9

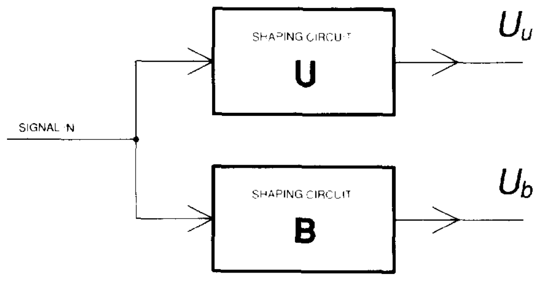


Fig. 1. Block diagram for the explanation of the operating principle.

$$F = Q_p/Q_t, \qquad (1)$$

and the ballistic deficit $B$ which is, by convention, defined as

$$B = 1 - F. \qquad (2)$$

For a given pulse shaping circuit the quantity $F$, and consequently $B$ also, is a function of the rise-time constant $\tau_r$ of the preamplifier output signal: $F = F(\tau_r)$ [1]. If $\tau_r$ depends on the type of the particle, by measuring $F$, one can discriminate between the different particles.

Let us consider two shaping circuits **B** and **U** resulting in a *different* ballistic deficit for the *same* input signal (see Fig. 1). The output signals reach their maxima at "peaking times" $T_{mb}(\tau_r)$ and $T_{mu}(\tau_r)$. Denoting these maxima by $U_b$ and $U_u$, respectively, one can create the ratio

$$P = \frac{U_b}{U_u}, \qquad (3)$$

which, supposing the gains for the two shaping circuits are the same, can be written as:

$$P = \frac{1 - B_b}{1 - B_u}. \qquad (4)$$

Here $B_b$ and $B_u$ are the ballistic deficits for circuits **B** and **U**, respectively. The quantity $P$ can also be used for particle discrimination, even if both $B_b$ and $B_u$ are particle ($\tau_r$) dependent but $B_b \neq B_u$, as we have supposed. In the following discussion we consider the special case of $B_u \approx 0$, for which determining $P$ is equivalent to measuring $F_b$ for circuit **B**:

$$P = 1 - B_b = F_b. \qquad (5)$$

For a given particle the quantity $P$ has a distribution around its mean value $\overline{P}$. The full width at half maximum (FWHM) $w$ of this distribution can be calculated from Eq. (3), which in general can be expressed in linear approximation, if $w \ll \overline{P}$, as:

$$w = \frac{1}{\overline{U}_u}\sqrt{v_b^2 + \overline{P}^2 v_u^2 - 2r\overline{P}v_b v_u}, \qquad (6)$$

where $\overline{U}_u$ is the mean value of $U_u$, and $r$ is the correlation coefficient between the output signal pairs $U_b$ and $U_u$ having FWHM $v_b$ and $v_u$, respectively. From Eq. (4) it is seen that $P$ does not depend on the signal amplitude, therefore if $\tau_r$ is independent of the particle energy, the $\overline{P}$ values for a given particle type of different energies lie on a horizontal line in a $P$ vs. energy $E$ plot. On the other hand, $w$ is inversely proportional to the signal amplitude (Eq. (6)), which means that on such a plot the points corresponding to the FWHM values lie on symmetric hyperbolas asymptotic to the average value of $P$.

For particles $x$ and $y$ e.g., which result in the same $U_{ux} = U_{uy}$ amplitude at the **U** output, the discrimination capability of a particle discriminator can be characterised by the figure of merit $M_{xy}$ [5] as follows:

$$M_{xy} = \frac{|\overline{P}_x - \overline{P}_y|}{w_x + w_y}, \qquad (7)$$

where $\overline{P}_i$ and $w_i$ ($i = x, y$ hereafter) are, respectively, the mean value and the FWHM of $P$ for particle $i$. In linear approximation for $B_b(\tau_r)$, using Eq. (5), we can write:

$$|\overline{P}_x - \overline{P}_y| = \left|\frac{dB_b(\tau_r)}{d\tau_r}\right| |\tau_{rx} - \tau_{ry}|, \qquad (8)$$

and substituting Eqs. (6) and (8) into Eq. (7) we obtain:

$$M_{xy} = \frac{D|\tau_{rx} - \tau_{ry}|}{\sum\limits_{i=x,y} \frac{\sqrt{v_{bi}^2 + (1 - B_{bi})^2 v_{ui}^2 - 2r_i(1 - B_{bi})v_{bi}v_{ui}}}{\overline{U}_{ui}(E_i)}}, \qquad (9)$$

where $\overline{U}_{ui}$ is the function of the particle energy $E_i$, and we introduced the dispersion $D$ defined by

$$D = \left|\frac{dB_b(\tau_r)}{d\tau_r}\right|. \qquad (10)$$

From Eq. (9) it can be established that, for a given pair of particles (i.e. for a given pair of $\tau_{rx}$ and $\tau_{ry}$), the figure of merit characterising the particle discrimination capability of the "ballistic deficit method" is proportional to the dispersion $D$ and to the energy of the incident particles, supposing that $\overline{U}_{ui}(E_i)$ is also proportional to the particle energy $E_i$. It can also be seen that a large value for $B_{bi}$, appearing in the denominator, also helps achieving a larger $M_{xy}$.

In the following we discuss the effect of $v_b$, $v_u$ and $r$ on the figure of merit. The signals $U_b$ and $U_u$, considered as stochastic variables, can be written as the sum of two independent terms, the corresponding detector signal $U_{dj}$, and the electronic noise $U_{nj}$ ($j = u, b$ hereafter),

$$U_j = U_{nj} + U_{dj}. \qquad (11)$$

[1] For the sake of simplicity in the following treatment only pulses of a single rise time constant $\tau_r$ are considered. For a detector signal composed of the sum of multiple $\tau_{ri}$ rise time constant components with relative intensities $q_i$ the resulting ballistic deficit will be the sum of the $B_i(\tau_{ri})q_i$ terms.

As a consequence both $v_b$ and $v_u$ also consist of two components:

$$v_j^2 = v_{nj}^2 + v_{dj}^2, \tag{12}$$

where $v_{nj}$ and $v_{dj}$ are, respectively, the FWHM of the noise at the output of the filters and of the detector signal, due to the statistical nature of the signal production in the detector. If the peaking time difference $(T_{mu} - T_{mb})$ has a large enough positive value, then $U_{nu}$ and $U_{nb}$ can also be considered as independent, but, since the two circuits process the *same* detector signal, $U_{du}$ and $U_{db}$ are *strongly correlated* according to the relationship

$$U_{du} = U_{db} + \delta U_{du}, \tag{13}$$

where $\delta U_{du}$ is related to the detector signal integrated in the time interval $(T_{mu} - T_{mb})$ and it is independent of $U_{db}$.

In practical applications the particle energy is widely used instead of the pulse amplitude, therefore in the following we introduce the energy equivalent of the above relations, taking into account that for energy dispersive detectors the signal amplitude is given by

$$U_i = K\frac{E_i}{\varepsilon_i}(1 - B_i), \tag{14}$$

where the coefficient $K$ accounts for the quantum and collection efficiency of the detector, the conversion of the preamplifier and the gain of the shaping amplifier. The quantity $\varepsilon_i(E_i)$, the average energy required to create one photon in scintillation detectors, one electron-hole pair in ionisation detectors, etc. depending on the type of the detector, can also be dependent on the type and the energy of the radiation as e.g. in scintillation detectors.

Using Eq. (12), for the energy resolution we obtain:

$$(\Delta E_j)^2 = (\Delta E_{nj})^2 + (\Delta E_{dj})^2, \tag{15}$$

where $\Delta E_{nj}$ and $\Delta E_{dj}$ are the electronic and detector contributions of the energy resolution, respectively. Note, that actually $\Delta E_{nj} = \Delta E_{nj}^0/(1 - B_j)$, where $\Delta E_{nj}^0$ refers to *zero* ballistic deficit. In the lack of an appropriate theory for $\Delta E_{dj}$ of the scintillation detectors, we shall use here an arbitrarily generalised empirical relationship, derived from the works [15-17] with the inclusion of the ballistic deficit, as

$$\Delta E_{dj} = \alpha[E(1 - B_j)]^\beta, \tag{16}$$

where $\alpha$ is a particle dependent constant, while $\beta \approx 0.25$-$0.28$ is independent of the type of the radiation (this is valid for $E_\gamma \geq 0.5$ MeV $\gamma$-rays, and for $E \geq 3$ MeV/amu p, d and $^3$He particles.)

In terms of energy Eqs. (6) and (9) can be rewritten as

$$w = \frac{P}{E}\sqrt{(\Delta E_b)^2 + (\Delta E_u)^2 - 2r\Delta E_b\Delta E_u}$$

$$= \begin{cases} \dfrac{P}{E}(\Delta E_b + \Delta E_u), & \text{if } r = -1, \\ \dfrac{P}{E}\sqrt{(\Delta E_b)^2 + (\Delta E_u)^2}, & \text{if } r = 0, \\ \dfrac{P}{E}|\Delta E_b - \Delta E_u|, & \text{if } r = 1 \end{cases} \tag{17}$$

and

$$M_{xy} = E_x D\,|\tau_{rx} - \tau_{ry}|\left[\sum_{i=x,y}\frac{\varepsilon_x}{\varepsilon_i}(1 - B_{bi}) \times\sqrt{(\Delta E_{bi})^2 + (\Delta E_{ui})^2 - 2r_i\Delta E_{bi}\Delta E_{ui}}\right]^{-1}, \tag{18}$$

respectively. In Eq. (17) the cases $r = -1, 0, 1$ correspond to anti-correlation, no correlation and full correlation.

The correlation coefficient $r$ is defined by

$$r = \frac{\overline{U_b U_u} - \overline{U_b}\,\overline{U_u}}{V(U_b)V(U_u)}, \tag{19}$$

where for the variance of $U_j$ we used the notation $V^2(U_j)$. A detailed calculation for $r$, using Eqs. (11)-(16), then gives:

$$r = (1 - B_b)\frac{(\Delta E_{db})^2}{\Delta E_b \Delta E_u}. \tag{20}$$

If $\Delta E_{db} = 0$ then $r = 0$, which corresponds to the case of $U_{nu}$ and $U_{nb}$ being independent. However, in practice neither $\Delta E_{db}$ nor $\Delta E_{du}$ is equal to zero, in which case

$$r = (1 - B_b)\left[1 + \left(\frac{\Delta E_{nb}^0/\Delta E_{db}}{1 - B_b}\right)^2\right]^{-1/2} \times\left[1 + B_b^{2\beta} + \left(\frac{\Delta E_{nu}^0/\Delta E_{du}}{(1 - B_b)^\beta}\right)^2\right]^{-1/2} \tag{21}$$

It can be seen that $0 < r < 1$, and for $\Delta E_{nj}/\Delta E_{dj} \ll 1$ the correlation coefficient $r$ can be approximated as

$$r = \frac{1 - B_b}{\sqrt{1 + B_b^{2\beta}}}. \tag{22}$$

### 2.2. Shaping circuits

As it can be seen from the preceding analysis the figure of merit of the ballistic deficit method is governed by the shaping circuits. Because of their simplicity the well known semi-Gaussian shapers are widely used in spectroscopic amplifiers. To realise the ballistic deficit pulse shape discrimination method we have also considered the application of such shapers.

As a first step we have determined both the ballistic deficit $B$ and the dispersion $D$ for such shapers. Unfortunately neither $B$ nor $D$ can be calculated in analytical form for practical circuits. Therefore we used the simulation program

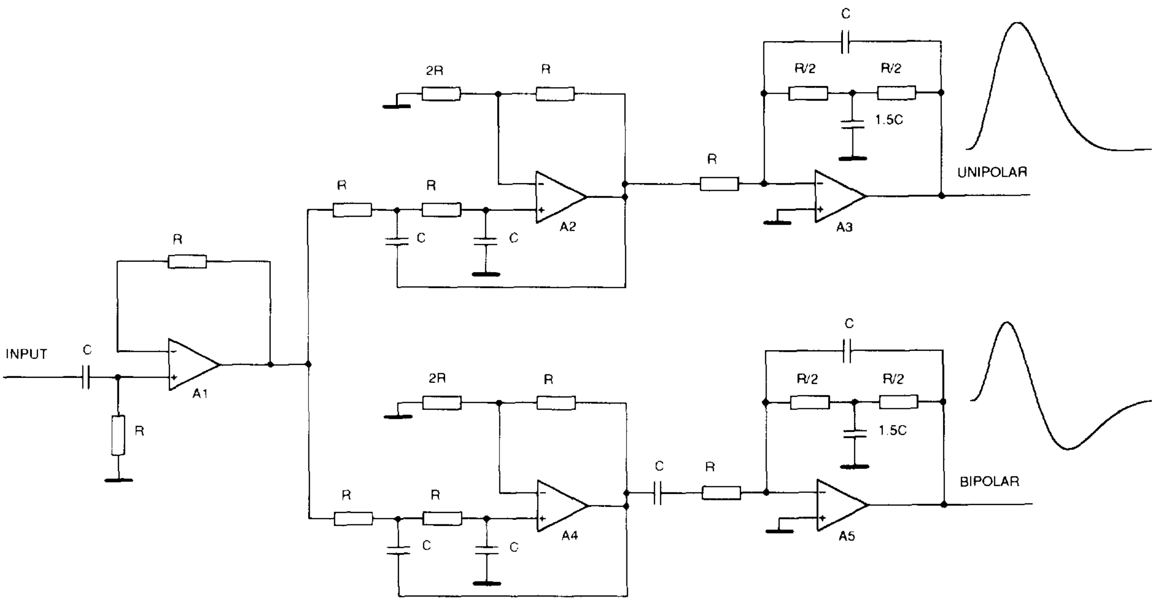


Fig. 2. Unipolar and bipolar filters used for ballistic deficit and dispersion calculations.

package SPICE for the numerical calculation of $B$ and $D$. The simplified circuitry of the unipolar and bipolar filters for which these calculations were performed are shown in Fig. 2. The results for $B$ and $D$ can be seen in Figs. 3a and 3b, respectively, as a function of the relative rise-time constant $T_r = \tau_r/\tau_s$, where $\tau_s$ is the shaping-time constant. It can be seen that for small $T_r$ values ($T_r < 0.1$) the ballistic deficit is negligible, while for large values ($T_r \geq 1$) $B$ is significant. Note also that for a pulse of a given rise time a unipolar filter has smaller ballistic deficit and dispersion than a bipolar one having the same shaping time constant. It can be seen from Fig. 3b. that the maximum value of $D$ for bipolar shaping is approximately 50% larger than that of $D$ for unipolar shaping.

These facts suggest choosing a unipolar filter for small-ballistic-deficit shaping (circuit **U**) and a bipolar one for large-ballistic-deficit shaping (circuit **B**), in order to achieve good particle discrimination by fulfilling the conditions mentioned in Section 2.1. If we want to approach the case corresponding to Eq. (5), for the filter **U** of Fig. 1 we have to use a unipolar filter with time constant large enough to diminish the ballistic deficit to a negligible level. Otherwise, referring to Eq. (9), for the shaper **B** it is a good choice to use a bipolar filter because of its large $D$. It is expedient to choose its time constant around the value corresponding to the maximum of $D$.

During the selection of the shaping time constant for the two filters it is not enough to deal with only $B$ and $D$. There are other conflicting factors, which have to be taken into consideration. From the point of view of the noise, for both

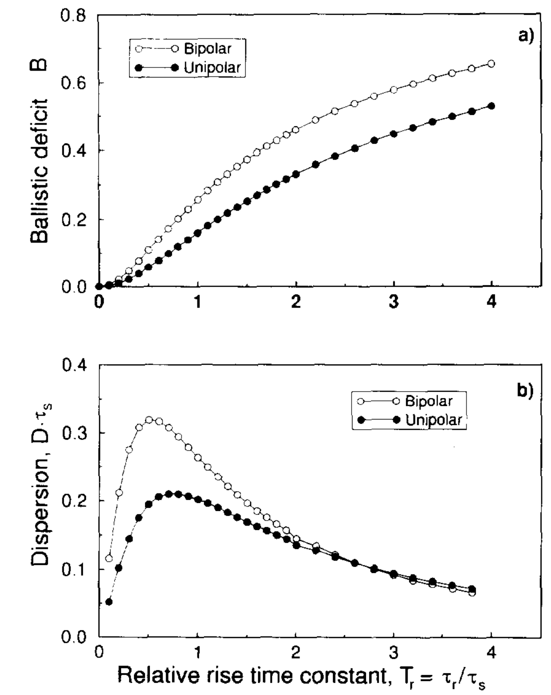


Fig. 3. (a) The ballistic deficit $B$ and (b) the dispersion $D$ vs. relative rise time constant $T_r$ for unipolar and bipolar shaping (see Fig. 2).

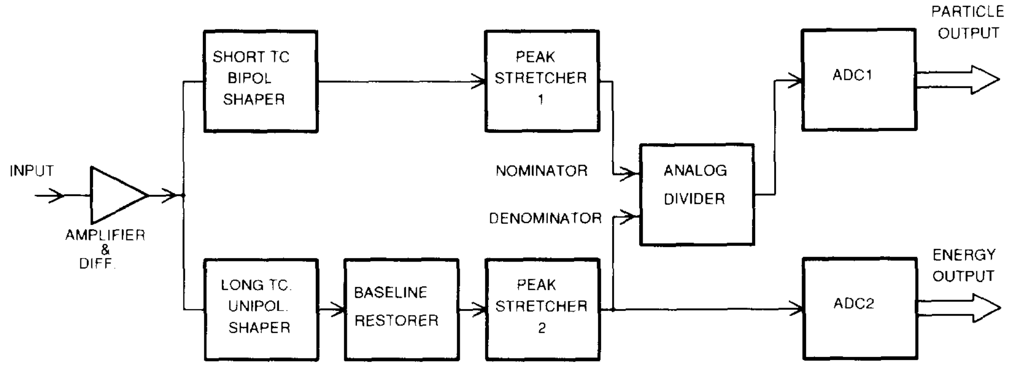


Fig. 4. Simplified block-diagram of the PDU.

filters, there is an optimum value for the shaping time constant. For the unipolar shaper, in order to reduce the ballistic deficit, we have to increase the shaping time constant. However, choosing the shaping time constant significantly larger than its optimum value, enhances the parallel noise contribution (i.e. $v_u$ increases), which originates mainly from the detector reverse current and the gate current of the FET in the charge sensitive preamplifier. At the same time a large shaping time constant results in a large dead time, thus reducing the maximum achievable count rate. In the case of the bipolar filter we have to increase the ballistic deficit by lowering the shaping time constant. Reducing this time constant below its optimum value, increases the series noise contribution (i.e. $v_b$ increases), consequently $M$ decreases (see Eqs. (9) and (18)). This implies that for $M$ the optimum value of the bipolar shaping time constant is larger than the value corresponding to the maximum of $D$. The series noise contribution is mainly governed by the FET transconductance and the capacitance at the preamplifier input (detector and stray capacitance). So choosing a FET with large transconductance and lowering the stray capacitance (e.g. by mounting the preamplifier directly to the detector instead of connecting them by long cables) can significantly improve $M$.

## 3. The particle discriminator

### 3.1. Overall description

The simplified block diagram of the PDU is shown in Fig. 4. The first stage is an amplifier including a short-time-constant differentiator (high pass filter). The output of the amplifier is connected simultaneously to the input of a long-time-constant unipolar shaper and to that of a short-time-constant bipolar shaper. The time constant of the unipolar shaper is chosen as a compromise between the negligible ballistic deficit and low parallel noise contribution. Its value was set to 10 $\mu$s. The time constant of the bipolar shaper is 1.2 $\mu$s which corresponds approximately to the maximum place of $D$. Choosing the unipolar and the bipolar filters for small and large ballistic deficit shaping, respectively, is also supported by the following facts: a) the energy resolution is superior for unipolar shaping, b) in the case of the bipolar shaping the baseline restorer can be omitted, c) the zero crossing point of the bipolar signal can be used as a time reference point.

The output of the bipolar shaper is fed directly through peak stretcher 1 to the nominator input of the analog divider. The unipolar shaper is followed by a baseline restorer which stabilizes the DC level and removes the low-frequency disturbances. Its output is led to peak stretcher 2 which supplies the denominator input of the analog divider and the energy signal. The analog divider produces the amplitude ratio of the bipolar and the unipolar signals, which ratio depends only on the particle type, since practically both signal amplitudes are proportional to the energy. Both the 'particle type' and the 'energy' analog signals are digitised by the analog-to-digital converters ADC1 and ADC2, respectively, which deliver eight-bit digital codes.

The acquisition of the data supplied by the ADCs can be realised in many different ways. For the results shown later data were stored in an incrementing matrix memory realised on a PC plug-in card. Plotting the 'particle type' output against the 'energy' output we got two-dimensional spectra, in which the points corresponding to the different types of particles are situated along different horizontal lines.

The system is also equipped with a counting type pile-up rejector (not shown in Fig. 4 for the sake of simplicity). It is part of a timing and logic unit which generates control signals for the stretchers and the ADCs. The timing signals, both leading edge and zero-crossing types, for this unit are extracted from the bipolar signal.

### 3.2. The amplifier

The simplified circuitry of the amplifier section is shown in Fig. 5. It consists of a differential input amplifier (realised

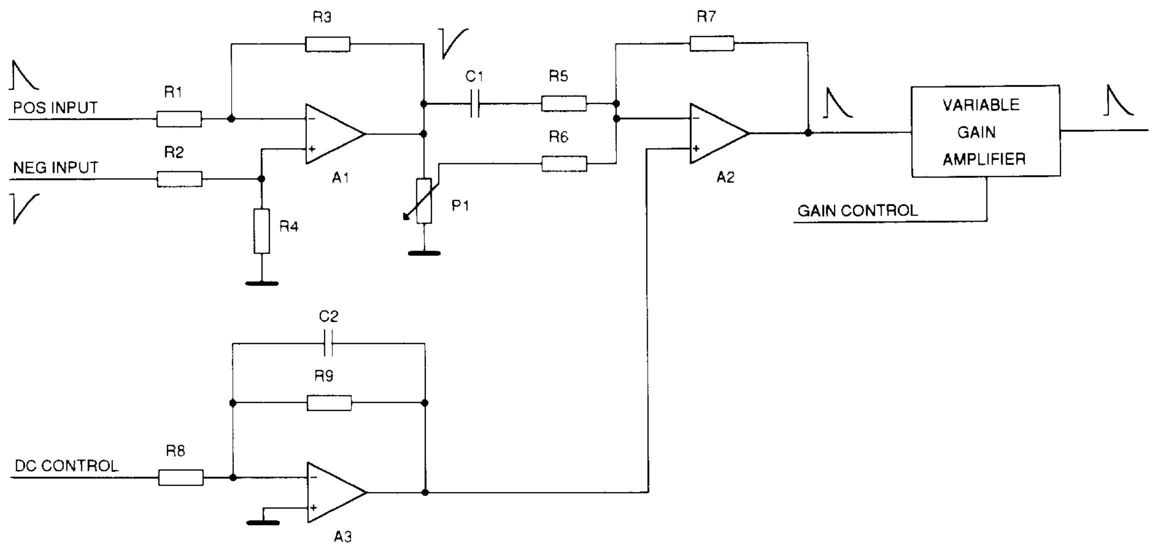


Fig. 5. Simplified circuitry of the amplifier section of the PDU.

by A1) for common mode noise suppression, followed by a pole-zero compensated differentiator (realised by A2). The time constant of the differentiator is equal to the short time constant shaping (in our case nominally 1.2 μs). The differentiated signals are further amplified by an amplifier, the gain of which can be controlled by a two-bit digital code. To preserve the rise time information of the input signal, this section is designed using high speed, fast slew rate current feedback operational amplifiers. The DC control amplifier (A3) sets the DC level at the output of the amplifier section to zero using a control signal delivered by the baseline restorer (see later).

### 3.3. The unipolar and bipolar shaper

The shapers realise similar transfer functions to those of the circuitry shown in Fig. 2. The high-pass filter part (the differentiator) is common for the unipolar and bipolar filters and it is situated in the amplifier section. Its shaping time constant is equal to that of the bipolar shaping (1.2 μs). Since the unipolar shaping time constant is 10 μs, the low-pass filter part of this shaper is preceded by a "pulse widening" circuit. Apart from this both the unipolar and bipolar shapers correspond to the circuit shown in Fig. 2. The gains of the different stages of both filters are chosen so that in the step response the amplitude of the unipolar pulse and the amplitude of the first lobe of the bipolar pulse will be equal.

### 3.4. The baseline restorer

The baseline restorer is shown in Fig. 6. The comparator CO senses the output of amplifier A, and compares it to the reference level set by potentiometer P. The current generators G1 and G2 deliver, respectively, currents $i_1$ and $i_2$ ($|i_2| > |i_1|$) into capacitor C. CO switches on and off G2 depending on whether the output of A is higher or lower than the reference level. This switching action of CO results in a stable DC level (equal to the reference level) at the output of A. At the same time on the capacitor C a compensating signal which is equal to the baseline shift and fluctuation is present. This compensating signal can be used to stabilise the DC level throughout the amplifier chain. This is realised by a feedback through the DC control amplifier (in the amplifier stage) which controls the DC level by resetting the compensating signal to zero on average. This kind of DC

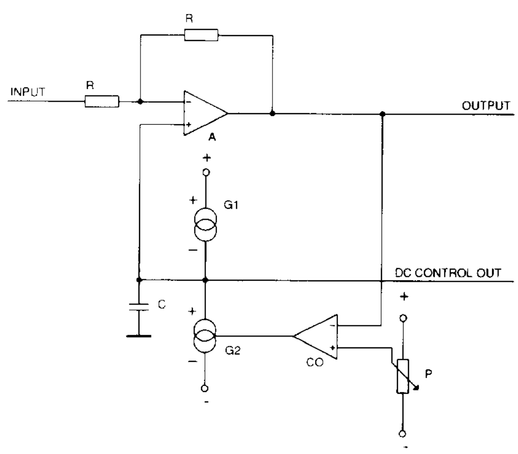


Fig. 6. Simplified circuitry of the baseline restorer.

level stabilization is very effective, and it can tolerate as large as $\pm 5$ V DC shift at the input of the PDU.

### 3.5. The stretchers

The amplitude maximum of both the unipolar and bipolar signals are stored in peak stretchers. Besides the analog input, the stretchers have two control inputs. One of them is for changing the tracking/stretching mode and the other one realises an inhibit/enable function. When a pulse arrives the stretcher is switched to stretching mode and after reaching the peak value of the signal, the stretcher is inhibited to accept another pulse. At the end of the signal processing period the stretcher is enabled and switched to tracking mode.

### 3.6. The analog divider

For making the ratio between the stretched bipolar and unipolar signals the analog divider Analog Devices AD734 is applied using its so-called direct denominator control feature.

### 3.7. The analog-to-digital converters

The analog-to-digital conversion is realised by monolithic analog-to-digital converters of successive approximation type (MAX162). The converters, which have a conversion time of 3 $\mu$s, make 12-bit conversion but only the 8 most significant bits are used as a conversion result. The 12-bit converter is chosen instead of an 8-bit one to assure an acceptable differential nonlinearity.

## 4. Experimental results

In this section some results are summarised, which were obtained from test experiments aimed at optimising the different parts and the overall performance of the PDU connected to a CsI(Tl) scintillator of $15\times15\times3$ mm$^3$ coupled to a S3590-03 Hamamatsu PIN photodiode via a 5 mm thick plexiglass lightguide [18]. Two types of experiments were carried out: a) Radioactive alpha and gamma sources and a random tail pulse generator were used to measure the effect of the shaping time constant used in the bipolar shaper and the effect of the detector capacitance on the figure of merit. b) The proton, $^3He^{2+}$ and $^4He^{2+}$ beams of the K=20 cyclotron accelerator of our institute in Debrecen were utilised to measure the energy dependence of the particle separation capability of the CsI+PIN diode detectors with this PDU.

### 4.1. Optimisation of the bipolar shaping

The discussion in Section 2.2 suggests that the figure of merit as a function of the bipolar shaping time constant has a maximum value. To check this and to experimentally find this maximum, the figure of merit was measured as a function of the shaping time constant for the bipolar shaper (see Fig. 2), using the $E_\gamma$ = 1.4 MeV line of a $^{152}$Eu gamma and the $E_\alpha$ = 4.8 MeV line of an AMR33 mixed alpha sources. The results shown in Fig. 7 prove the existence of such a maximum, and in the PDU the bipolar shaping time constant has been fixed at $\tau_s = 1.2$ $\mu$s.

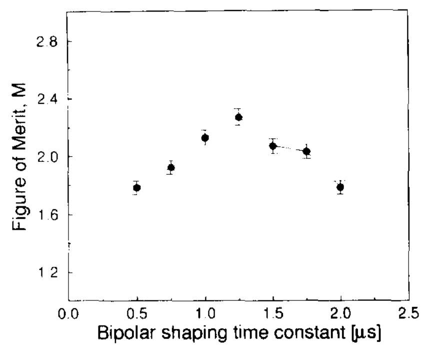


Fig. 7. The measured figure of merit vs. shaping time constant used for optimising the bipolar shaper.

### 4.2. Effect of the input capacitance

In order to study the effect of the external capacitance at the preamplifier input, the figure of merit was measured when coupling additional capacitances parallel to the CsI detector. In Fig. 8 the figure of merit is shown as a function of the excess capacitance coupled to the capacitance of the PIN diode itself, which was 50 pF. This figure can be used to evaluate the effect of the cable length connecting the detector to the preamplifier (see also the discussion at the end of Section 2).

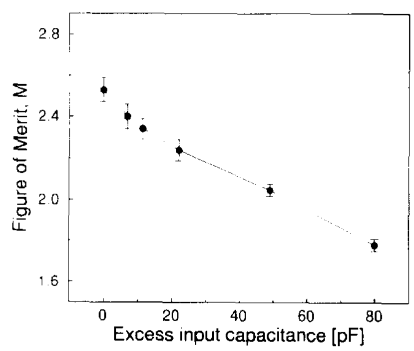


Fig. 8. Figure of merit measured for 1.4 MeV gammas and 4.8 MeV alpha particles as a function of the excess capacitance added in parallel to the capacitance of the PIN photodiode.

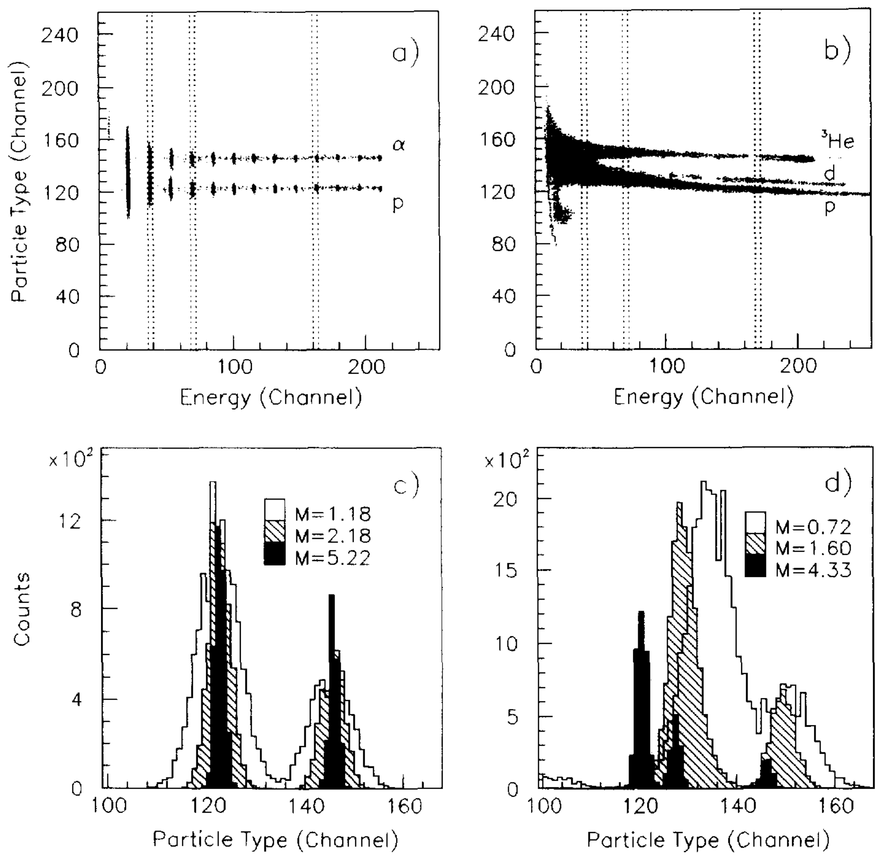


Fig. 9. 'Particle type vs. energy' plots for (a) pulse generator simulated protons and alphas, and (b) for particles measured in nuclear reaction $^{12}C+^{3}He$ at $E$ = 20 MeV. Vertical cuts (c) and (d) taken at different energies indicated by dotted vertical stripes in matrices (a) and (b), respectively, to illustrate the separation of different particles. The figure of merit $M$ is also shown for each cut denoted in different shadings.

### 4.3. Particle separation

After optimising the different parts of the particle discriminator unit (PDU), the particle separation capability of the CsI + PDU system was also tested by measuring the figure of merit as a function of the particle energy. In Fig. 9. the results of different experiments are compared. Protons and alpha particles were simulated by a random tail pulse generator using pulses with different rise times which correspond to the decay times of the 'proton' and 'alpha' light in CsI(Tl). The horizontal distributions shown in Fig. 9a reflect that no "energy" dependence in the rise times appears in this case. For real protons and alphas, originating from nuclear reactions (Fig. 9b), the proton line bends towards the alpha line at low energies. This indicates that at lower energies the dependence of the rise time on the proton energy will be a limiting factor for the low-energy threshold in the particle separation of the system. The figure of merits calculated by taking vertical cuts (Figs. 9c and 9d) in the 'particle type-energy' matrices are shown in Fig. 10. The solid line stands for the case of the pulse generator, while different symbols correspond to $^4$He–proton, proton–deuteron and $^3$He–proton pairs of particles. For all cases an almost linear energy dependence is obvious in accordance with Eq. (18). Particle separation is possible down to figure of merit $M \approx 0.6$, giving a low-energy separation threshold at around $E_\alpha \approx 4$ MeV and $E_p \approx 2.5$ MeV.

## 5. Summary

The experimental tests show that the ballistic deficit method is a very good alternative for particle discrimination with CsI(Tl) detectors. Although we have tried this technique with this type of detectors, there are no any limiting factors to use it with other detectors for any kind of pulse shape discrimination purposes. The advantage of this method is that techniques which are well proved in the

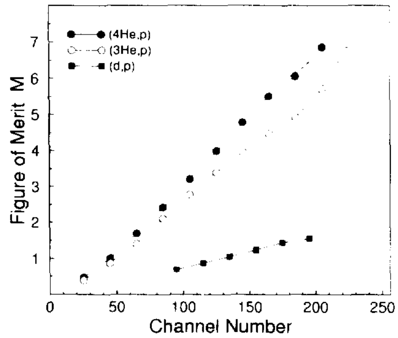


Fig. 10. Figure of merit $M$ measured for simulated proton–alpha pair (solid line) and for real $^4$He-proton, $^3$He-proton and proton–deuteron pairs (symbols) as function of the particle energy.

pulse-amplitude spectroscopy (shaping, baseline restoration, etc.) can be used directly without any alteration. As for the particle separation capability of the PDU for protons and alphas, according to the measured figure of merit, these two types of particles can be discriminated down to energies $E_p \approx 2.5$ MeV and $E_\alpha \approx 4$ MeV, using CsI(Tl) detectors. Even deuterons are well separated from protons. Due to the specific circuitry, the PDU also supplies high-resolution particle energy information, which would enable more complex analysis in special applications. The low separation limit, the almost parallel particle distributions in the particle vs. energy plots achieved with our particle discriminator using CsI(Tl)+PIN-diode detectors, make the PDU useful in most nuclear physics applications where the selection of certain reaction products is based on the discrimination of the light charged particles. For example, in the study of very neutron deficient nuclei by large $\gamma$-ray detector arrays, like the planned EUROBALL system, the use of an internal CsI(Tl) detector array coupled with such PDUs helps the enhancement of very weak reaction channels by proper gating on such a particle matrix and by selecting the required particle multiplicity.

## Acknowledgements

This work was supported in part by the Swedish National Research Council and by the Hungarian Scientific Research Fund (OTKA) under contract No. T7481 and A293.

## References

[1] J. Alarja, A. Dauchy, A. Giorni, C. Morand, E. Pollaco, P. Stassi, R. Billerey, B. Chambon, B. Cheynis, D. Drain and C. Pastor, Nucl.Instr. and Meth. A 242 (1986) 352.

[2] F. Benrachi, B. Chambon, B. Cheynis, D. Drain, C. Pastor, D. Seghier, K. Zaid, A. Giorni, D. Heuer, A. Llères, C. Morand, P. Stassi and J.B. Viano, Nucl. Instr. and Meth. A 281 (1989) 137.

[3] J. Gál, G. Hegyesi, G. Kalinka, B.M. Nyakó, G.E. Perez, A. Kerek and A. Johnson, Nucl. Instr. and Meth. A (submitted for publication).

[4] L. Koch, Y. Koechlin, B. Mougin, L. Treguer, Nuclear Electronics Vol. 1 (International Atomic Energy Agency, Vienna) p. 54.

[5] R. A. Winyard, J. E. Lutkin and G. W. McBeth, Nucl. Instr. and Meth. 95 (1971) 141.

[6] R. Fülle, Gy. Máthé and D. Netzband, Nucl. Instr. and Meth. 35 (1965) 250.

[7] F.D. Brooks, Nucl. Instr. and Meth. 4 (1959) 151.

[8] J.C. Robertson and A. Ward, Proc. Phys. Soc. (London) 73 (1959) 523.

[9] M.G. Strauss and R.N. Larsen, Nucl. Instr. and Meth. 56 (1967) 80.

[10] G. Kalinka, EUROBALL Meeting on Auxiliary Detectors and Selective Devices, Berlin, June 1–3, 1992, Slides Report.

[11] Z. He, A.J. Bird and D. Ramsden, Nucl. Instr. and Meth. A 336 (1993) 236.

[12] E. Baldinger and W. Franzen, Adv. in Electron. and Electron Physics 8 (1956) 255.

[13] P.W. Nicholson, Nuclear Electronics (Wiley, London, 1974).

[14] B.W. Loo, F.S. Goulding and D. Gao, IEEE Trans. Nucl. Sci. NS-35 (1988) 114.

[15] G.G. Kelley, P.R. Bell, R.C. Davis and N.H. Lazar, Nucleonics 14 (1956) 53; and I.R.E. Trans. Nucl. Sci. NS-13 (1956) 57.

[16] H. Grassmann, H.G. Moser, H. Dietl, G. Eigen, V. Fonseca, E. Lorenz and G. Mageras, Nucl. Instr. and Meth. A 234 (1985) 122.

[17] V.V. Avdeichikov, L. Bergholt, M. Guttormsen, J.E. Taylor, L. Westerberg, B. Jakobsson, W. Klamra and Yu. Murin, Nucl. Instr. and Meth. A 394 (1994) 216.

[18] G. Kalinka et al., to be published.